C Journal of Carbon Research

MDPI

Article

Carbon-Based Magnetic Nanocarrier for Controlled Drug Release: A Green Synthesis Approach

Jessica R. P. Oliveira [1,2], Raquel O. Rodrigues [1,3], Lillian Barros [1], Isabel C. F. R. Ferreira [1], Luís F. Marchesi [2], Martina Koneracka [4], Alena Jurikova [4], Vlasta Zavisova [4] and Helder T. Gomes [1,3,*]

1 Centro de Investigação de Montanha (CIMO), Instituto Politécnico de Bragança, Campus de Santa Apolónia, 5300-253 Bragança, Portugal; joliveira@ipb.pt (J.R.P.O.); raquel.rodrigues@ipb.pt (R.O.R.); lillian@ipb.pt (L.B.); iferreira@ipb.pt (I.C.F.R.F.)
2 Department of Chemical Engineering, Universidade Tecnológica Federal do Paraná, Av. Monteiro Lobato, s/n–Jardim Carvalho, Ponta Grossa, PR 84016-210, Brasil; luismarchesi@gmail.com
3 Laboratory of Separation and Reaction Engineering—Laboratory of Catalysis and Materials (LSRE-LCM), Faculdade de Engenharia, Universidade do Porto, Rua Dr. Roberto Frias, 4200-465 Porto, Portugal
4 Institute of Experimental Physics, Slovak Academy of Sciences, Watsonova 47, 040-01 Košice, Slovak Republic; konerack@saske.sk (M.K.); akasard@saske.sk (A.J.); zavisova@saske.sk (V.Z.)
* Correspondence: htgomes@ipb.pt; Tel.: +351-273303110

Received: 15 November 2018; Accepted: 22 December 2018; Published: 28 December 2018

check for updates

Abstract: In this study, hydrophilic magnetic nanoparticles were synthesized by green routes using a methanolic extract of *Rubus ulmifolius* Schott flowers. The prepared magnetic nanoparticles were coated with carbon-based shell for drug delivery application. The nanocomposites were further chemically functionalized with nitric acid and, sequentially, with Pluronic® F68 (CMNPs-plur) to enhance their colloidal stability. The resulting material was dispersed in phosphate buffer solution at pH 7.4 to study the Doxorubicin loading. After shaking for 48 h, 99.13% of the drug was loaded by the nanocomposites. Subsequently, the drug release was studied in different working phosphate buffer solutions (i.e., PB pH 4.5, pH 6.0 and pH 7.4) to determine the efficiency of the synthesized material for drug delivery as pH-dependent drug nanocarrier. The results have shown a drug release quantity 18% higher in mimicking tumor environment than in the physiological one. Therefore, this study demonstrates the ability of CMNPs-plur to release a drug with pH dependence, which could be used in the future for the treatment of cancer "in situ" by means of controlled drug release.

Keywords: green routes; magnetic nanoparticles; drug delivery; cancer therapy; doxorubicin

1. Introduction

In the last decades, nanomaterials have been extensively studied for different applications in order to explore their enhanced properties acquired at the nanoscale. For biomedical applications, there is a demand to synthesize nanomaterials with optimized and combined features, such as biocompatibility, colloidal stability, high specific surface area, and controlled shape and size, among others. To fulfill this demand, a multidisciplinary approach is required, uniting several scientific fields, such as biomedicine, chemical, physics, engineering, biology and pharmaceutical [1]. These nanomaterials can be developed for combined biomedical applications, such as medical diagnosis and therapy, including target drug delivery [2], magnetic resonance imaging (MRI) [3] and cancer hyperthermia treatment [1,4], which has increased their interest for nanomedicine. Several methods to synthesize these nanomaterials have been developed to find some alternatives that are applicable, efficient and with minimal side effects. The most common used methods of synthesis are microemulsion, thermal decomposition, solvothermal, sonochemical, microwave-assisted, chemical vapor deposition, combustion synthesis, carbon arc, laser pyrolysis synthesis, co-precipitation and green routes [5,6].

Green synthesis are alternative and environmental friendly ways to synthesize magnetic nanoparticles (MNPs) [7,8], consisting on the use of plant extracts with reducing power. Typically, green synthesis is made only by adding the plant extract in a solution containing Fe (III) and/or Fe (II) at room temperature and stirring for a given time [9–14]. However, to obtain nanoparticles (NPs) with the desired size, the reaction temperature must be well controlled [7,15–17]. Since this methodology does not use many reagents and do not discard harmful components in the washing step, this synthesis received the name of green synthesis or green routes. Also, there is the possibility of using a concentrated basic solution added to the mixture of iron solution with vegetal extract [6,8,18]. Nevertheless, in general, bare iron oxide magnetic nanoparticles have low biocompatibility to cells and due to their high magnetic interaction, they tend to aggregate and to form clots.

In this study, to suppress these drawbacks, MNPs synthesized by green route were coated with carbon-based shells. Generally, these carbon-based nanocomposites have high surface area, are chemically inert, biocompatible, thermally stable and electrically conductive [19], desirable for biomedical applications. In addition to coating, the carbon-based magnetic nanoparticles (CMNPs) were functionalized with nitric acid and Pluronic® F-68 (CMNPs-plur) to enhance the colloidal stability by the incorporation of carboxylic acid and polymer groups on the carbon-based shell.

The resultant CMNPs-plur are negatively charged, enabling them to have great affinity with cationic drugs, such as doxorubicin hydrochloride (DOX). This drug has been used successfully to produce regression in various neoplasms, such as breast cancer, lung, bladder, thyroid and ovary carcinoma, soft tissue sarcoma and bone sarcoma, Hodgkin's and non-Hodgkin's lymphomas, neuroblastoma, Wilms' tumor, acute lymphoblastic leukemia and acute myeloblastic leukemia [20]. The electrostatic interaction between both can be different in solutions with different pH. Such difference can facilitate both the drug loading and the drug release depending on the solution that will be used.

The pH-dependent drug release is very important due to the difference between the pH of the normal tissues (pH 7.4), the extracellular environment of the tumor (pH 6.5) and the endosome and lysosome (pH 5.0) [21]. Therefore, if more drug is released in the more acidic environment, the treatment of the tumor will be improved and the side effects and damage to the healthy cells will be lower. Accordingly, the main objective of this work was the development and optimization of smart magnetic nanostructures coated with carbon materials with high potential for the cancer treatment through the pH-dependent controlled release of drugs.

2. Materials and Methods

2.1. Chemicals and Plant Samples

The reagents used for the research were: Ammonia solution 25% (Applichem-Panreac, Darmstadt, Germany); disodium hydrogen phosphate dodecahydrate ($Na_2HPO_4 \cdot 12H_2O$, Centralchem, Bratislava Slovakia); doxorubicin hydrochloride (DOX, Discovery Fine Chemicals, Wimborne, U.K.); ethanol absolute (Fisher Scientific, Loughborough, U.K.); formaldehyde (37–38% *w/w*, Panreac, Barcelona, Spain); iron (II) chloride tetrahydrate ($FeCl_2 \cdot 4H_2O$, Sigma-Aldrich, Germany); iron (III) chloride hexahydrate pure ($FeCl_3 \cdot 6H_2O$, Applichem-Panreac, Darmstadt, Germany); Pluronic® F-68 (Sigma-Aldrich, Germany); sodium dihydrogen phosphate hydrate ($NaH_2PO_4 \cdot H_2O$, Centralchem, Bratislava, Slovakia); resorcinol (Fisher Scientific, Loughborough, U.K.); sodium hydroxide solution (NaOH, Fisher Scientific, Loughborough, U.K.); tetraethyl orthosilicate (TEOS, Fluka Cheika, Germany).

Rubus ulmifolius Schott flowers, *Tamus communis* L. shoots and *Crateagus monogyna* Jacq. flowers were collected in the Natural Park of Montesinho territory, Trás-os-Montes, North-eastern Portugal, as previously described [22–24].

2.2. Methods

For a better understanding of the process, the following flowchart represents the steps of the used methodology, Figure 1. Those steps will be described in detail in sequence.

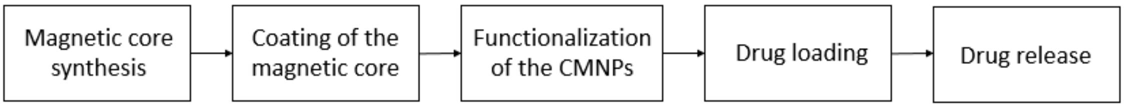

Figure 1. Flowchart of the process.

2.2.1. Extracts Preparation

Each plant sample (1 g) was macerated with 30 mL of methanol at 25 °C, 150 rpm, for 1 h. The extract was filtered through Whatman n° 4 paper and the residue was then re-extracted with an additional portion of 30 mL of methanol. The combined extracts were evaporated at 35 °C (rotary evaporator Büchi R-210) to remove methanol and to obtain dry extracts.

2.2.2. Magnetic Core Synthesis and Coating

The magnetic core was synthesized according to the methodology described by Awwad & Salem (2012) [6], i.e., using a solution of Fe(II) and Fe(III). Briefly, 0.53 g of $FeCl_2 \cdot 4H_2O$ and 1.11 g of $FeCl_3 \cdot 6H_2O$ (1:2 molar ratio) were dissolved in 100 mL of distilled water. The vessel containing this solution was placed in an oil bath on a magnetic stirring plate (IKA® C-MAG HS 7 with temperature control IKA® ETS-DS)) until 30 °C was reached, and at this temperature, 5 mL of plant extract was added [6]. The extract concentration was 100 times higher than the EC_{50} RP (EC_{50} Reducing Power) concentration, i.e. the extract concentration was calculated from the method of Oyaizu (1986) to determine reducing power [25,26]. The EC_{50} values correspond to the extract concentration that provides 50% of reducing power or antioxidant activity. The lower the EC_{50} values means the higher the antioxidant capacity of the samples. Different plant methanolic extracts with high reducing power were investigated in the synthesis of magnetic cores, such as *R. ulmifolius* flowers (EC_{50} RP 40 $\mu g \cdot mL^{-1}$, which corresponds to the sample concentration providing 0.5 of absorbance, in the reducing powder assay), *T. communis* shoots (EC_{50} RP 68 $\mu g \cdot mL^{-1}$) and *C. monogyna* flowers (EC_{50} RP 19 $\mu g \cdot mL^{-1}$) [22,24]. After 5 min, 30 mL of ammonium hydroxide, 1 M (from ammonia solution 25% diluted) were added dropwise to the mixture using a peristaltic pump (ISM 845, ISMATEC). The solution remained in stirring for 1 h at 30 °C. A representation of this synthesis methodology can be observed in Figure 2. The solution was washed with distilled water by centrifugation at 6000 rpm for 5 min (MPW-260R centrifuge, MPW Med. Instruments). The washing process was repeated 7 times. Finally, the last washing was done with ethanol and then the MNPs were dried at 60 °C in a drying oven (Binder FD 115).

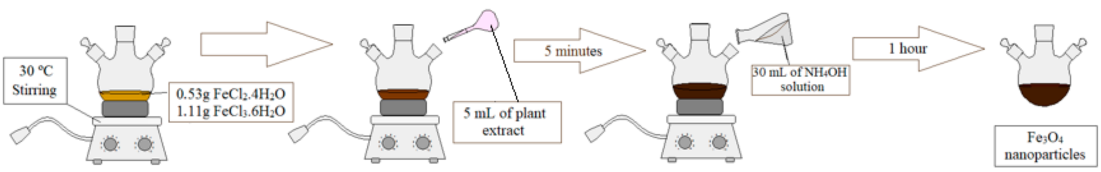

Figure 2. Magnetic core synthesis methodology.

The magnetic core resulting from these three plant extracts was characterized by X-ray diffraction (XRD) and Transmission Electron Microscopy (TEM) in order to perform phase identification, determine the crystalline structure and the total core size. XRD analysis was performed in a PANalytical X'Pert MPD equipped with a X'Celerator detector and secondary monochromator (Cu Kα λ = 0.154 nm; data recorded at a 0.017° step size). The composition of magnetite present was identified using

HighScore software and Crystallography Open Database. Rietveld refinement of the XRD diffraction patterns was performed using PowderCell software allowing phase quantification. Crystallite sizes were determined by the Williamson-Hall method [27]. TEM was performed in a Transmission Electron Microscope LEO 906E instrument operating at 120 kV, equipped with a 4 Mpixel 28 × 28 mm Charge-Coupled Device (CCD) camera from TRS [27]. ImageJ software (1.46r, NIH, Bethesda, MD, USA) was used to estimate the size of the magnetic nanoparticles.

The protocol proposed by Liu et. al. (2014) was used to produce the carbon-based coating. At the first step, 0.25 g of magnetic nanoparticles synthesized by the method previously described were suspended in 150 mL of ethanol and 50 mL of distilled water. The mixture was ultrasonicated for 45 min (Ultrasons-H, P-Selecta) and then the solution was poured into a 500 mL round bottom flask with 0.1 g of resorcinol and 1.4 mL of ammonia solution (25%). The mixture was remained in stirring for 1 h at 30 °C in an oil bath on a magnetic stirring plate with temperature control. In the second step, 0.15 mL of formaldehyde solution (37−40%) and 0.205 mL of tetraethyl orthosilicate (TEOS) solution were added dropwise and the mixture was stirred for 6 h at the same temperature. After that, the mixture was heated at 80 °C for 8 h under stirring. The resultant solid sample was washed 7 times with distilled water by centrifugation at 6000 rpm for 5 min. Finally, having done the last washing with ethanol absolute, the MNPs were dried at 60 °C in the drying oven. The resultant NPs were denoted Fe_3O_4@polymer [19,28].

At the second step of the coating process, the Fe_3O_4@polymer sample was carbonized under a N_2 atmosphere in a vertical tubular furnace (ROS 50/250/12, Thermoconcept). The carbonization occurred up to 600 °C at a heating rate of 1 °C·min^{-1} and the temperature was maintained at 600 °C for 3 h. The resultant NPs were etched under stirring with sodium hydroxide solution (10 mol·L^{-1} for 24 h at room temperature) and the product was washed by centrifugation with distilled water several times, until reaching pH 7. In the last step, the sample was washed with ethanol and dried at 60 °C in a drying oven [19,28] (CMNPs).

2.2.3. Functionalization

The colloidal stability of as-synthesized CMNPs was enhanced by the chemical oxidation of carbon-based shell at mild acid treatment followed by the incorporation of Pluronic® F-68, with the conditions shown in Figure 3. For chemical oxidation, CMNPs were treated with nitric acid solution (1 mol·L^{-1}) at 60 °C for 3 h under stirring with temperature control. The product of the reaction was washed by centrifugation at 6000 rpm for 5 min. The washing process was repeated several times with distilled water, and one more time with ethanol absolute, then the sample was dried at 60 °C in a drying oven.

Afterwards, 20 mg of CMNPs functionalized in nitric acid and 203.2 mg of Pluronic® F-68 was weighed, and resuspended in 20 mL of ultrapure water. This sample was sonicated in Branson Digital Sonifier® for 30 min in pulsed mode (15 s on and 15 s off). Then, the solution was maintained in a shaker (Bioshake IQ, Qinstruments, Jena, Germany) for 3 h, at 25 °C and 6000 rpm. In sequence, nanoparticles were washed three times with ultrapure water in ultracentrifuge (Sorvall Discovery M120 SE, Thermo Fisher Scientific Inc., Waltham, MA, USA) at 25 °C and 25,000 rpm, for 30 min. Finally, the NPs were dispersed in 5 mL of ultrapure water (CMNPs-plur).

Both the Zeta potential and DLS measurements were performed with 5 µL of the solution CMNPs-plur (4 mg·mL^{-1}) diluted in 1 mL of ultrapure water in Zetasizer NanoZS equipment. The measurements were analyzed by Zetasizer software. The magnitude of the Zeta potential indicates the degree of electrostatic repulsion between adjacent, similarly charged particles in a dispersion and is a key indicator of colloidal suspension stability, as well. For molecules and particles that are small enough, a high Zeta potential will confer stability, so the solution or dispersion will resist aggregation [29].

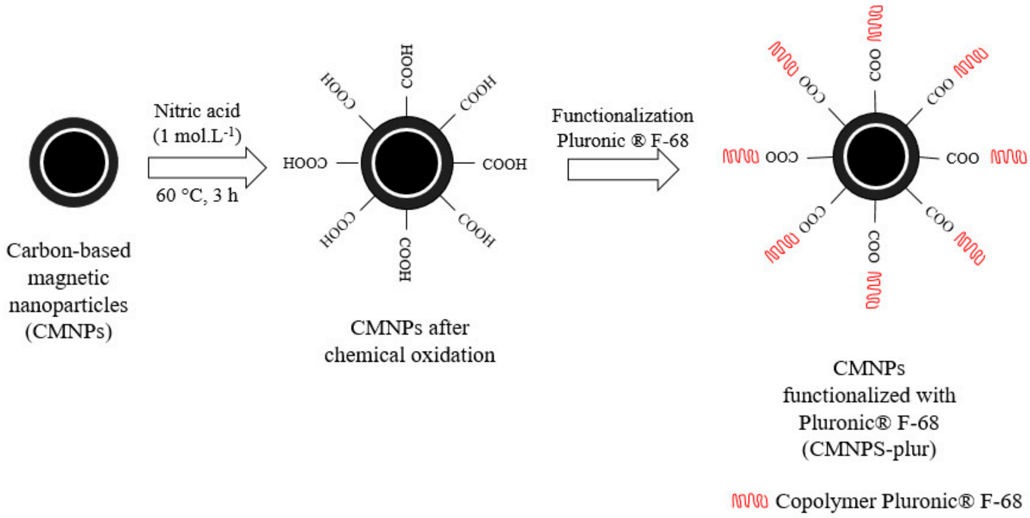

Figure 3. Scheme of superficial change after functionalization from CMNPs to CMNPs-plur.

2.2.4. Drug Loading and Release

Phosphate buffers (PB) with different pH were used to assess the efficiency of the developed nanosystem as pH-dependent drug nanocarrier. These solutions with pH 6.0 and 7.4 were prepared according to Promega Protocol & applications guide, using $Na_2HPO_4 \cdot 12H_2O$ and $NaH_2PO_4 \cdot H_2O$ [30]. The PB at pH 4.5 was prepared using 0.05 M of the $NaH_2PO_4 \cdot H_2O$ solution.

The DOX loading in CMNPs functionalized with Pluronic® F-68 (CMNPs-plur) was performed as follows: 20 mg of CMNPs-plur was firstly dissolved in 5 mL of ultrapure water and then corrected to final volume of 20 mL with PB pH 7.4. Then, the solution was sonicated in ultrasonic bath (Ultrasonic Compact cleaner 1 L, Powersonic PS01000A, NOTUS, Vrable, Slovakia) for 1 h. The DOX solution was prepared by dissolving 20 mg of Doxorubicin in 5 mL of ultrapure water and then corrected to 20 mL with PB pH 7.4. This solution was placed on magnetic stirrer until a homogeneous solution was obtained. Next, both CMNPs-plur and DOX solutions were mixed together and placed in orbital shaker for 48 h at room temperature with stirring (100 rpm). In sequence, each sample was centrifuged 2 times at 8000 rpm for 10 min. To calculate the concentration of the DOX loaded on CMNPs-plur, the supernatants were measured at 480 nm in a UV-VIS spectrometer (Specord 40, Analytik Jena AG, Jena, Germany). DOX loaded concentration was calculated as difference between theoretical input DOX loading and DOX concentration in supernatant. The loading was expressed in terms of drug loading capacity (DLC) and drug loading efficiency (DLE).

The pH-dependence release test was made in triplicate at different pH: PB pH 4.5, PB pH 6.0 and PB pH 7.4. Around 3 mg of freeze-dried carbon-based nanoparticles functionalized with Pluronic® F-68 containing Doxorubicin (CMNPs-plur-DOX), were weighed and 1 mL of each buffer solution were added in each flask. The flasks were placed in the orbital shaker, at 37 °C and after 15 min of shaking, the mixture was centrifuged and supernatant was measured by UV-Vis spectrophotometry at 480 nm to identify the concentration of the DOX that was released in each solution. This process of centrifugation and analysis of the supernatant was repeated in times of 15 min, 30 min, 1 h, 2 h, 3 h, 4 h, 24 h, 48 h and 72 h. From the collected data, a curve of the concentration released over time was plotted to analyze the difference of the drug release at different pH [31].

3. Results and Discussion

3.1. Magnetic Core Synthesis and Coating

The synthesis of the magnetic cores was performed with three different plant extracts, namely *R. ulmifolius* flowers, *Tamus communis* L. shoots and *Crateagus monogyna* Jacq. flowers, which were compared among themselves. The three types of core exhibit magnetic properties and have black color. The yields of MNPs were very similar 516 mg, 501 mg and 416 mg, respectively. However, visibly, the more stable magnetic core in distilled water was observed in case of *R. ulmifolius* flowers extract used for magnetic core synthesis, Figure 4.

Figure 4. Colloidal stability of the magnetic cores in distilled water with extracts of *R. ulmifolius* flowers, *T. communis* shoots and *C. monogyna* flowers, from left to right respectively.

The XRD spectrum of the magnetic core nanoparticles are presented in Figure 5. The peaks at 30.62°, 35.75°, 43.37°, 53.70°, 57.38°, 63.06° and 74.37° are attributed to the crystal planes of the magnetic cores at 220, 311, 400, 422, 511, 440 and 533, respectively. The relative intensity of the diffraction peaks fits with the standard XRD data for magnetite (JCPDS no. 19-0629). Therefore, the investigation of phase by XRD confirms the crystal structure of the three cores synthesized as magnetite. Moreover, the core with *R. ulmifolius* flowers extract has particle size of 13.5 ± 1.0 nm, while the cores with *T. communis* shoots and *C. monogyna* flowers extract have particle sizes of 12.3 ± 0.6 nm and 12.8 ± 0.5 nm, respectively.

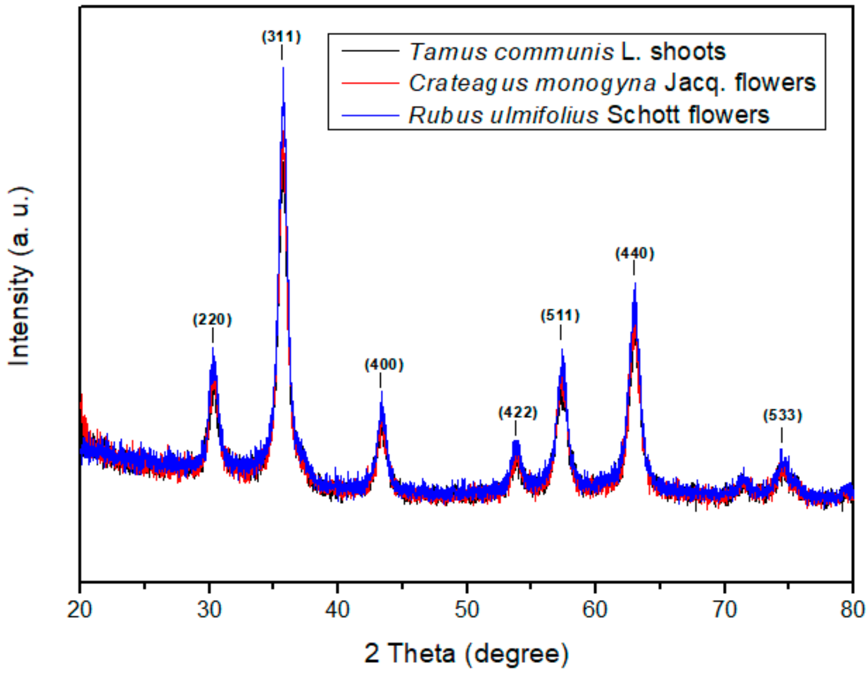

Figure 5. XRD patterns of the magnetic cores synthesized with *R. ulmifolius* flowers, *T. communis* shoots and *C. monogyna* flowers extracts.

Since the best colloidal stability of the magnetic core was obtained with the *R. ulmifolius* flowers extract, this synthesis method was chosen to continue in the next experiments. In its extract, twenty-four phenolic compounds can be identified, such as phenolic acid derivatives (di- and caffeoylquinic acids, *p*-coumaroylquinic acids, feruloylquinic acids and ellagic acid), flavonoids (quercetin and kaempferol glycoside derivatives and catechin) and hydrolysable tannins (lambertianin, sanguiin and four di-hexahydroxydiphenol (HHDP)- galloyl glucose isomers) [25]. For the green routes synthesis, the flavonoids are probably involved in the stages of initiation of nanoparticle formation and further aggregation, in addition to the bioreduction stage, mainly due to the presence of various functional groups capable of nanoparticle formation [17]. Besides the composition and reducing power of the extract, the methodology adopted uses ammonium hydroxide to perform the synthesis of the magnetite core by the chemical precipitation method.

TEM image presented in Figure 6a shows the bare magnetite core synthesized with *R. ulmifolius* flowers extract with average size of 13.4 $\pm$ 3.5 nm. The observed agglomeration is related to the magnetic characteristics of the sample. Figure 6b shows the TEM images of the carbon-based magnetic nanoparticles after coating, which resulted in particles with average sizes of 20.2 $\pm$ 8.7 nm.

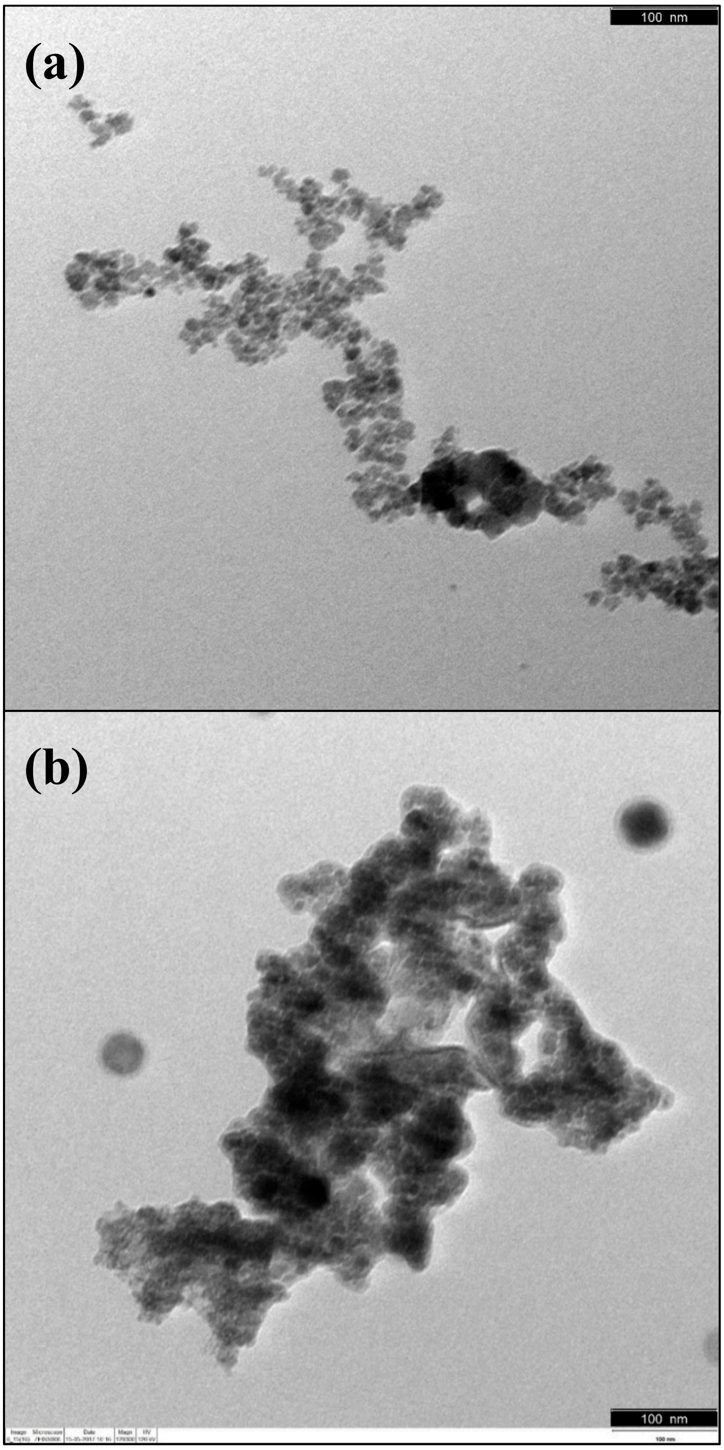

Figure 6. TEM image of the: (**a**) Bare magnetite core synthesized with *R. ulmifolius* flowers extract; (**b**) sample resulted from the coating processes. Scale bar represents 100 nm.

3.2. Functionalization

The functionalization with nitric acid added various oxygen-containing functional groups, such as carboxylic acid groups (−COOH) to the CMNPs structures, increasing the acidity of the nanocomposites. The spectral analysis measured by means of Fourier transform infrared spectrometer (FT-IR), Figure 7, shows the comparison of the nanocomposite spectra before and after functionalization. The presence of magnetite in non-functionalized CMNPs, as well as in functionalized CMNPs is confirmed by the absorption bands of 564 cm^{-1}, 1628 cm^{-1} and 3433 cm^{-1}. The first band corresponds to the vibration of the Fe–O bond, and the latter two can be attributed to the bending and stretching vibrations of the surface –OH present in the carbon-based shell [32]. The absorption bands at 1380 cm^{-1}, 1458 cm^{-1}, 1627 cm^{-1}, 2923 cm^{-1} and 3433 cm^{-1} represent the C–O, O–H, C=O, C–H and O–H bonds respectively, which indicate various oxygen-containing functional groups in the samples, including hydroxyl (C–OH) carboxyl (COOH) and ketonic (C=O) species. Both spectra show similar behavior. However, it is possible to observe the loss of hydroxyl groups (3433 cm^{-1}) and Fe-O (564 cm^{-1}) after functionalization. The latter it could indicate oxidation in the magnetic core. Therefore, this indicates the increase of the carboxyl groups, which are responsible for making the nanocomposites more acidic. The presence of carboxyl groups in nanocomposites is ascribed to the enhancement of their colloidal stability and monodispersibility in aqueous solutions [33].

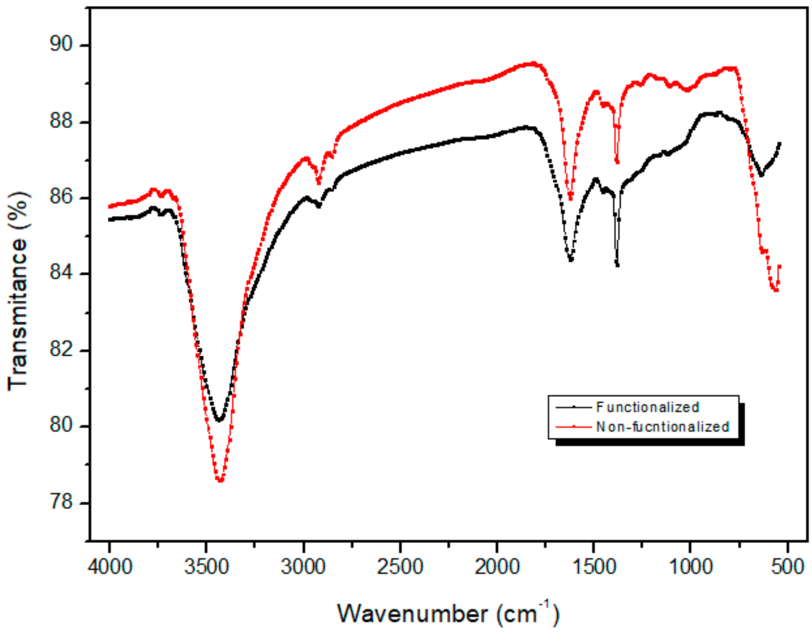

Figure 7. Fourier transform infrared spectrometer (FT-IR) absorption bands of functionalized and non-functionalized CMNPs.

In addition to the incorporation of oxygen-groups on the carbon-based shell by using nitric acid, another functionalization was performed using Pluronic® F-68 to enhance the colloidal stability of the nanocomposites in aqueous salty medium. To fully characterize the final nanomaterial, additional characterizations of CMNPs-plur were performed, such as: measurement of Zeta potential (Zetasizer Nano ZS, Malvern, UK), size distribution by measurement of Dynamic Light Scattering (DLS; Zetasizer Nano ZS, Malvern, UK), magnetic properties by using Magnetic Property Measurement System 5XL (MPMS, Quantum Design, CA, USA), thermogravimetric analysis (TGA, Differential Thermal and Thermogravimetric Analyser-TGDTA SETSYS 16, Setaram, France) and Scanning Electron Microscopy (SEM; JEOL7000F microscope).

The result of the Zeta potential measurement showed the magnitude -22.1 ± 4.1 mV for CMNPs-plur sample (Figure 8b). The negative charge observed in the material can be explained by two main factors: the incorporation of carboxylic acid groups (via acid treatment) and the previously reported associated negative charge of materials functionalized with Pluronic [28,34,35], resulting in a consequent increase of the colloidal stability. In addition, the negative surface charge is attributed to the increased circulation of nanoparticles. This fact would be positive in future in vitro cellular applications, since it may avoid the phenomenon of opsonization (a process by which the plasma immunoproteins bind to the surface of the particle leading to elimination of nanoparticles by macrophages) [28,36].

Moreover, the negative charge of the studied nanoparticles, which is advantage for the combination of this material with the cationic drug Doxorubicin (which has NH_3^+ group). The DLS results showed the average hydrodynamic diameter (D_H) of CMNPs-plur sample approximately to 396 nm with polydispersity index (PDI) of 0.27, Figure 8a. The low PDI value demonstrates the uniformity of hydrodynamic size of the nanoparticles in the sample.

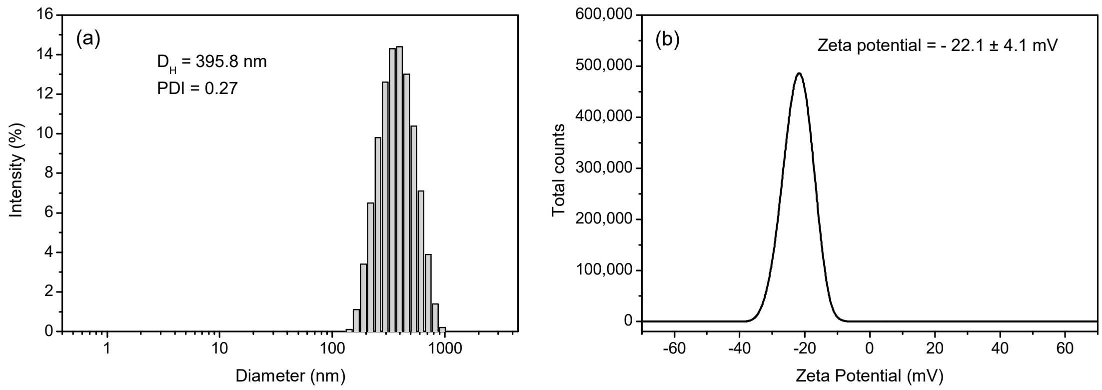

Figure 8. Size distribution obtained by DLS (**a**) and Zeta potential (**b**) of the CMNPs-plur sample.

The superparamagnetic nanoparticles have unique domain. In a simple approximation, the total magnetic moment of the nanoparticle can be considered as a very high magnetic moment, composed of all the individual magnetic moments of the atoms that form the nanoparticle. The superparamagnetic behavior is characterized by a typical relaxation time, which refers to the time required for the systems to obtain zero magnetization after an external magnetic field is removed [34,35]. The superparamagnetism allied to a high saturation magnetization also allows the use of MNPs for magnetic hyperthermia based in the heat generated by magnetic samples in the presence of an AC magnetic field and for cancer treatment as well. The magnetic properties of the CMNPs-plur sample were measured by SQUID magnetometer. As it can be seen in Figure 9, superparamagnetic behavior was registered at 300 K. The sample did not exhibit hysteresis, and neither coercivity nor remanence was detected. The saturation magnetizations of the CMNPs-plur sample was found to be 64.49 emu·$g^{-1}{}_{magnetite}$. Moreover, having fitted of the first quadrant of hysteresis loop by Langevin function, the magnetic core diameter was calculated. The distribution of magnetic core diameter is seen in Figure 9, right inset. The calculated value (D_{MAG} = 12.1 nm) is in good agreement with the results from XRD and TEM.

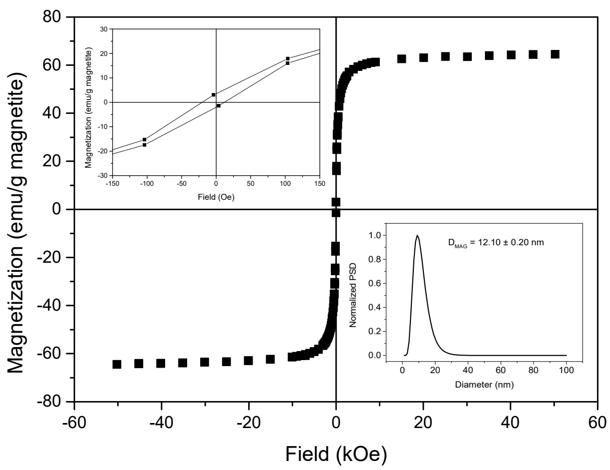

Figure 9. Magnetic hysteresis curve of CMNPs-plur sample and magnetic core size distribution obtained from magnetic measurements (right inset).

To determine the amount of individual components (magnetite, carbon and Pluronic® F-68) in the CMNPs-plur sample TGA was carried out. Thermogravimetric curves representing decomposition of the different stages of the total process, namely bare magnetite, CMNPs, CMNPs-plur, as well as Pluronic, are shown in Figure 10. Only little weight loss up to 100 °C, related to the humidity of all analyzed samples (about 6%), was observed. The difference in weight losses obtained by comparing the CMNPs with the magnetite samples was 9% and it is related to the carbon coating. The weight loss approximately 56% corresponding to Pluronic was obtained by comparison of CMNPs-plur with CMNPs thermograms. Considering that all Pluronic is decomposed at 800 °C and magnetite as inorganic compound shows thermal stability (in the measured temperature range), then the remaining weight of 29% corresponds to the amount of magnetite in the CMNPs-plur sample used on the drug loading and release tests.

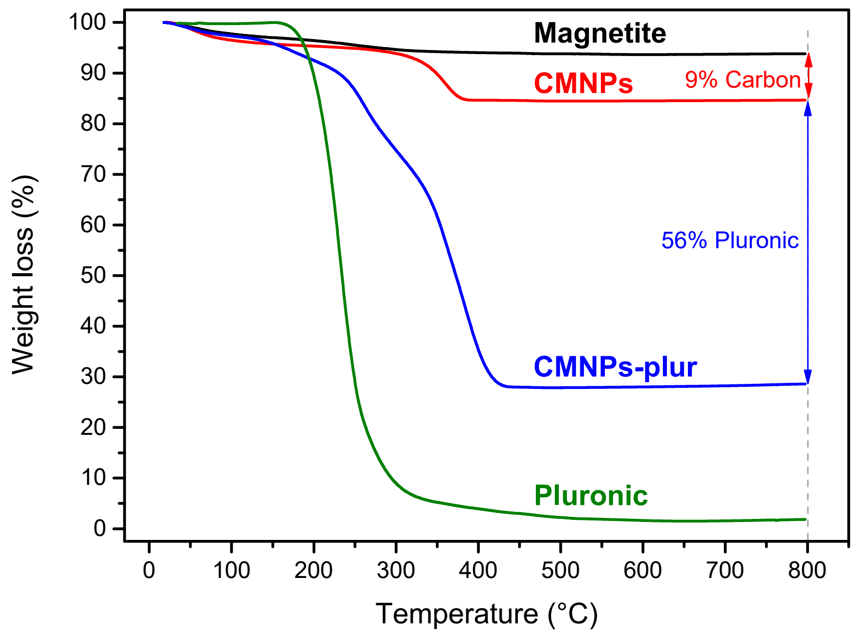

Figure 10. Thermograms of the magnetite, CMNPs, CMNPs-plur and Pluronic.

For the study of morphology and size of prepared samples, Scanning Electron Microscopy (SEM, JEOL7000F, JEOL Lda., Tokyo, Japan) was used. The samples for observations were prepared as follows: 20 µL of 50-times diluted sample CMNPs-plur was placed as drop on an aluminum disc and after evaporation of the water and sputtering with carbon the sample was observed by SEM. The SEM image of CMNPs-plur is in Figure 11. The CMNPs-plur have an average particle diameter of approximately 58.0 ± 17.0 nm. This considerable increase in size may be a consequence of the reaction between the nanoparticles surface functional groups with Pluronic® F-68, by which it is possible to form polymer aggregates around some sets of nanoparticles.

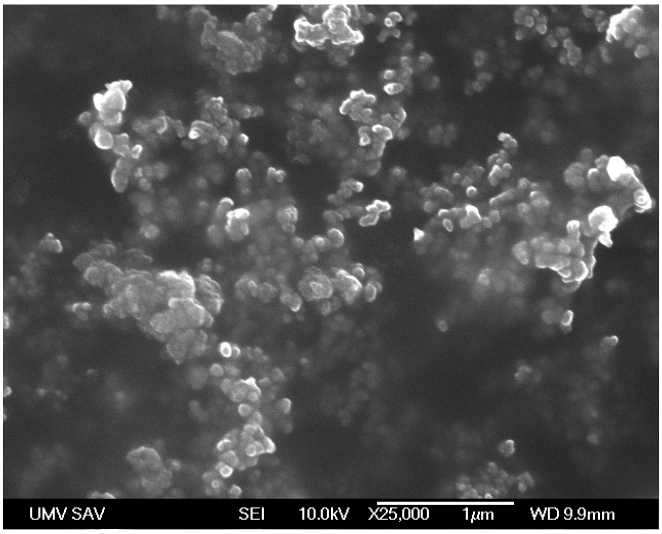

Figure 11. SEM image of CMNPs-plur.

3.3. Drug Loading and Release

Initially, the DLC ($\mu g \cdot \mu g^{-1}$) and DLE (%) were calculated using the DOX concentration in the supernatant measured by the UV-VIS spectrometer:

$$\mathrm{DLC} = \frac{\mathrm{C_{DOX-CMNPs-plur}}}{\mathrm{C_{CMNPs-plur}}} \tag{1}$$

$$\mathrm{DLE}(\%) = \frac{\mathrm{C_{iDOX}} - \mathrm{C_{fDOX}}}{\mathrm{C}_{0DOX}} * 100 \tag{2}$$

where, $C_{\text{DOX-CMNPs-plur}}$ is concentration of DOX loaded in the CMNPs-plur, $C_{\text{CMNPs-plur}}$ is concentration of CMNPs-plur, C_{iDOX} is initial concentration of DOX before loading, C_{fDOX} is final concentration of DOX in supernatant after loading. The results of drug loading are 0.991 $\mu g \cdot \mu g^{-1}$ and 99.1%, to DLC and DLE, respectively.

The pH dependent release is very important due to the difference between the pH of the normal tissues (pH 7.4), the extracellular environment of the tumor (pH 6.5) and the endosome and lysosome (pH 5.0) [21]. Therefore, if more drug is released in the more acidic environment, the treatment of the tumor could be more efficient and side effects and damage of the healthy cells could be lower. Interestingly, the drug release test revealed higher drug deliver in acidic medium. The *in vitro* results show that the cumulative drug release (%) of DOX after 72 h were 19.3%, 4.4% and 1.5%, which represent a DOX mass of 287 μg, 67 μg and 23 μg, in PB solutions with pH 4.50, pH 6.0 and pH 7.5, respectively. The drug release over time is represented in Figure 12, the standard deviation for each pH was very small, between 0.01 and 0.25. Therefore, it is possible to evaluate that this material has good reproducibility in the drug release tests.

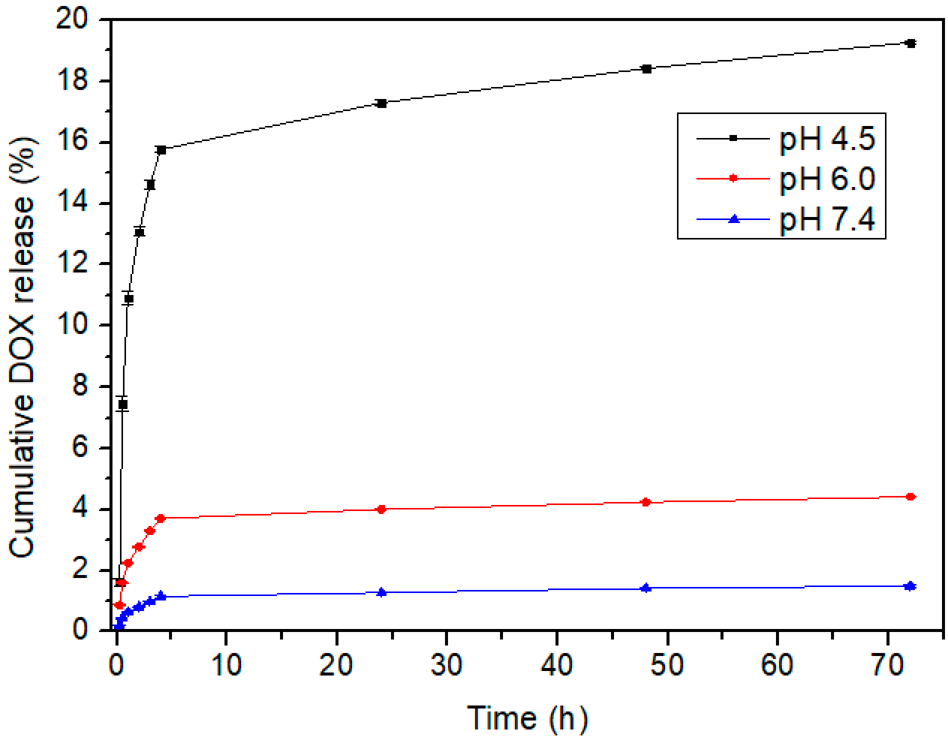

Figure 12. Drug release in percentage of DOX over time at 37 °C.

The results of drug release reveal that the nanocarriers have a dependent response to the pH of the medium, releasing more DOX at mimic tumoral conditions, i.e., pH 4.5, than at physiological ones, pH 7.4. The main reasons for this phenomenon comes from the π–π stacking interactions between the carbon-based nanostructures and the aromatic DOX molecules, which can be easily disrupted under a mild acidic environment, as well as due to the increased solubility of DOX caused by the protonation process [28]. In this case, this pH-dependent controlled release can be also ascribed to the increased protonation of the nanocarrier surface as the pH of the aqueous solution decreases from 7.4 to 4.5, with the associated loss of negative surface charge. This will lead to a reduction of the electrostatic attraction between CMNPs-plur and DOX protonated molecules, increasing the progressive drug release [28].

4. Conclusions

The use of plant extracts in the synthesis of magnetic compounds have been explored due to their content in phenolic compounds. The polyphenols via green routes are able to reduce the iron ions to magnetite, which enables the formation of colloidal magnetic cores, by the incorporation of phenolic groups, i.e., flavonoids. Improved colloidal stability enables the individual coating of the magnetic nanomaterial to single core-shell and not clusters of magnetite with carbon. Drug loading and release tests performed with CMNPs-plur revealed the ability to use this nanocomposite as pH-dependent drug nanocarriers. Impressively, the synthesized nanocomposite showed an outstanding drug loading of 99.1%. On the other hand, the final release was approximately 18% higher in solution at mimicked acidic tumor environment than in a solution at pH equivalent to normal cells (physiological pH). Therefore, the carbon-based magnetic nanocarriers functionalized with Pluronic® F-68 have one possible application in the treatment of cancer by means of the pH-dependent controlled release. Another possible clinical application to be explored is the potential of this nanomaterial for the synergistic effect of drug delivery and hyperthermia. Due to its superparamagnetic behavior and high magnetic saturation, this nanomaterial may have the ability to act in combination for those two treatments in the cancer therapy.

Author Contributions: Conceptualization, R.O.R. and H.T.G.; Data curation, M.K.; Formal analysis, L.F.M.; Investigation, J.R.P.O. and L.B.; Methodology, R.O.R.; Project administration, H.T.G.; Resources, I.C.F.R.F., V.Z. and H.T.G.; Supervision, L.F.M. and H.T.G.; Validation, V.Z. and A.J.; Writing—original draft, J.R.P.O.; Writing—review & editing, R.O.R., L.B., I.C.F.R.F., M.K. and H.T.G.

Funding: This research was funded by: Project POCI-01-0145-FEDER-006984 – Associate Laboratory LSRE-LCM funded by FEDER through COMPETE2020 - POCI – and by national funds through FCT (Fundação para a Ciência e a Tecnologia); RTChip4Theranostics, supported by Programa Operacional Regional do Norte—Norte Portugal Regional Operational Programme (NORTE 2020), under the PORTUGAL 2020 Partnership Agreement, through the European Regional Development Fund (ERDF) and by FCT.

Acknowledgments: The authors are grateful to FCT, and FEDER under Programme PT2020 for financial support to CIMO (UID/AGR/00690/2013) and L. Barros contract. R.O.R. acknowledges the Ph.D. scholarship SFRH/BD/97658/2013 granted by FCT. This work was also supported by the Slovak Scientific Grant Agency projects VEGA 2/033/19.

Conflicts of Interest: The authors declare no conflict of interest.

References

1. Teja, A.S.; Koh, P. Synthesis, properties, and applications of magnetic iron oxide nanoparticles. *Prog. Cryst. Growth Charact. Mater.* **2009**, *55*, 22–45. [CrossRef]
2. Mohapatra, S.; Rout, S.R.; Das, R.K.; Nayak, S.; Ghosh, S.K. Highly Hydrophilic Luminescent Magnetic Mesoporous Carbon Nanospheres for Controlled Release of Anticancer Drug and Multimodal Imaging. *Langmuir* **2016**, *32*, 1611–1620. [CrossRef] [PubMed]
3. Sun, C.; Lee, J.S.H.; Zhang, M. Magnetic Nanoparticles in MR Imaging and Drug Delivery. *Adv. Drug Deliv. Rev.* **2009**, *60*, 1252–1265. [CrossRef] [PubMed]
4. Zamora-Mora, V.; Fernández-Gutiérrez, M.; González-Gómez, Á.; Sanz, B.; Román, J.S.; Goya, G.F.; Hernández, R.; Mijangos, C. Chitosan nanoparticles for combined drug delivery and magnetic hyperthermia: From preparation to in vitro studies. *Carbohydr. Polym.* **2017**, *157*, 361–370. [CrossRef] [PubMed]
5. Faraji, M.; Yamini, Y.; Rezaee, M. Magnetic nanoparticles: Synthesis, stabilization, functionalization, characterization, and applications. *J. Iran. Chem. Soc.* **2010**, *7*, 1–37. [CrossRef]
6. Awwad, A.M.; Salem, N.M. A green and facile approach for synthesis of magnetite nanoparticles. *J. Nanosci. Nanotechnol.* **2012**, *2*, 208–213. [CrossRef]
7. Shah, S.; Dasgupta, S.; Chakraborty, M.; Vadakkekara, R.; Hajoori, M. Green synthesis of iron nanoparticles using plant extracts. *Int. J. Biol. Pharm. Res.* **2014**, *5*, 549–552.
8. Yew, Y.P.; Shameli, K.; Miyake, M.; Kuwano, N.; Bahiyah, N.; Khairudin, A.B.; Mohamad, S.E.B.; Lee, K.X. Green synthesis of magnetite (Fe_3O_4) nanoparticles using seaweed (*Kappaphycus alvarezii*) extract. *Nanoscale Res. Lett.* **2016**, *11*, 1–7. [CrossRef]
9. Harshiny, M.; Iswarya, C.N.; Matheswaran, M. Biogenic synthesis of iron nanoparticles using *Amaranthus dubius* leaf extract as a reducing agent. *Powder Technol.* **2015**, *286*, 744–749. [CrossRef]
10. Wang, Z.; Fang, C.; Mallavarapu, M. Characterization of iron-polyphenol complex nanoparticles synthesized by Sage (*Salvia officinalis*) leaves. *Environ. Technol. Innov.* **2015**, *4*, 92–97. [CrossRef]
11. Makarov, V.V.; Makarova, S.S.; Love, A.J.; Sinitsyna, O.V.; Dudnik, A.O.; Yaminsky, I.V.; Taliansky, M.E.; Kalinina, N.O. Biosynthesis of stable iron oxide nanoparticles in aqueous extracts of Hordeum vulgare and *Rumex acetosa* plants. *Langmuir* **2014**, *30*, 5982–5988. [CrossRef] [PubMed]
12. Martínez-Cabanas, M.; López-García, M.; Barriada, J.L.; Herrero, R.; Sastre de Vicente, M.E. Green synthesis of iron oxide nanoparticles. Development of magnetic hybrid materials for efficient As(V) removal. *Chem. Eng. J.* **2016**, *301*, 83–91. [CrossRef]
13. Machado, S.; Pacheco, J.G.; Nouws, H.P.A.; Albergaria, J.T.; Delerue-Matos, C. Characterization of green zero-valent iron nanoparticles produced with tree leaf extracts. *Sci. Total Environ.* **2015**, *533*, 76–81. [CrossRef] [PubMed]
14. Mahdavi, M.; Namvar, F.; Ahmad, M.; Mohamad, R. Green biosynthesis and characterization of magnetic iron oxide (Fe_3O_4) nanoparticles using seaweed (*Sargassum muticum*) aqueous extract. *Molecules* **2013**, *18*, 5954–5964. [CrossRef] [PubMed]
15. Prasad, C.; Gangadhara, S.; Venkateswarlu, P. Bio-inspired green synthesis of Fe_3O_4 magnetic nanoparticles using watermelon rinds and their catalytic activity. *Appl. Nanosci.* **2016**, *6*, 797–802. [CrossRef]

16. Wang, T.; Lin, J.; Chen, Z.; Megharaj, M.; Naidu, R. Green synthesized iron nanoparticles by green tea and eucalyptus leaves extracts used for removal of nitrate in aqueous solution. *J. Clean. Prod.* **2014**, *83*, 413–419. [CrossRef]
17. Iravani, S. Green synthesis of metal nanoparticles using plants. *Green Chem.* **2011**, *13*, 2638–2650. [CrossRef]
18. Al-kalifawi, E.J. Green synthesis of magnetite iron oxide nanoparticles by using Al-Abbas's (A.S.) Hund Fruit (*Citrus medica*) var. *Sarcodactylis Swingle* extract and used in Al-'alqami river water treatment. *J. Nat. Sci. Res.* **2015**, *5*, 125–135.
19. Liu, W.; Liu, Y.; Yan, X.; Yong, G.; Xu, Y.; Liu, S. One-pot synthesis of yolk-shell mesoporous carbon spheres with high magnetisation. *J. Mater. Chem. A* **2014**, *2*, 9600–9606. [CrossRef]
20. Righetto, L. *Doxorrubicina—Bula Doxorrubicina*. 2013. Available online: https://www.4medic.com.br/bulario/D/doxorrubicina/ (accessed on 6 September 2018).
21. Du, J.-Z.; Du, X.-J.; Mao, C.-Q.; Wang, J. Tailor-made dual pH-sensitive polymer-doxorubicin nanoparticles for efficient anticancer drug delivery. *J. Am. Chem. Soc.* **2011**, *133*, 17560–17563. [CrossRef]
22. Barros, L.; Oliveira, S.; Carvalho, A.M.; Ferreira, I.C.F.R. In vitro antioxidant properties and characterization in nutrients and phytochemicals of six medicinal plants from the Portuguese folk medicine. *Ind. Crops Prod.* **2010**, *32*, 572–579. [CrossRef]
23. Barros, L.; Carvalho, A.M.; Ferreira, I.C.F.R. Comparing the composition and bioactivity of *Crataegus Monogyna* flowers and fruits used in folk medicine. *Phytochem. Anal.* **2011**, *22*, 181–188. [CrossRef] [PubMed]
24. Martins, D.; Barros, L.; Carvalho, A.M.; Ferreira, I.C.F.R. Nutritional and in vitro antioxidant properties of edible wild greens in Iberian Peninsula traditional diet. *Food Chem.* **2011**, *125*, 488–494. [CrossRef]
25. Martins, A.; Barros, L.; Carvalho, A.M.; Santos-Buelga, C.; Fernandes, I.P.; Barreiro, F.; Ferreira, I.C.F.R. Phenolic extracts of *Rubus ulmifolius Schott* flowers: Characterization, microencapsulation and incorporation into yogurts as nutraceutical sources. *Food Funct.* **2014**, *5*, 1091–1100. [CrossRef] [PubMed]
26. Ferreira, I.C.F.R.; Baptista, P.; Vilas-Boas, M.; Barros, L. Free-radical scavenging capacity and reducing power of wild edible mushrooms from northeast Portugal: Individual cap and stipe activity. *Food Chem.* **2007**, *100*, 1511–1516. [CrossRef]
27. Ribeiro, R.S.; Rodrigues, R.O.; Silva, A.M.T.; Tavares, P.B.; Carvalho, A.M.C.; Figueiredo, J.L.; Faria, J.L.; Gomes, H.T. Hybrid magnetic graphitic nanocomposites towards catalytic wet peroxide oxidation of the liquid effluent from a mechanical biological treatment plant for municipal solid waste. *Appl. Catal. B Environ.* **2017**, *219*, 645–657. [CrossRef]
28. Rodrigues, R.O.; Baldi, G.; Doumett, S.; Garcia-Hevia, L.; Gallo, J.; Bañobre-López, M.; Dražić, G.; Calhelha, R.C.; Ferreira, I.C.F.R.; Lima, R.; et al. Multifunctional graphene-based magnetic nanocarriers for combined hyperthermia and dual stimuli-responsive drug delivery. *Mater. Sci. Eng. C* **2018**, *93*, 206–217. [CrossRef]
29. Das, C.; Bose, S. *Advanced Ceramic Membranes and Applications*; CRC Press: New York, NY, USA, 2017.
30. Promega Buffers for Biochemical Reactions. *Protoc. Appl. Guid.* Available online: https://worldwide.promega.com/resources/product-guides-and-selectors/protocols-and-applications-guide/buffers-for-biochemical-reactions/ (accessed on 25 October 2018).
31. Rodrigues, R.; Baldi, G.; Doumett, S.; Gallo, J.; Bañobre-López, M.; Dražić, G.; Calhelha, R.; Ferreira, I.; Lima, R.; Silva, A.; et al. A Tailor-made protocol to synthesize yolk-shell graphene-based magnetic nanoparticles for nanomedicine. *J. Carbon Res.* **2018**, *4*, 16. [CrossRef]
32. Bagavathi, M.; Ramar, A.; Saraswathi, R. Fe_3O_4–carbon black nanocomposite as a highly efficient counter electrode material for dye-sensitized solar cell. *Ceram. Int.* **2016**, *42*, 13190–13198. [CrossRef]
33. Wang, H.; Chen, Q.-W.; Chen, J.; Yu, B.-X.; Hu, X.-Y. Carboxyl and negative charge-functionalized superparamagnetic nanochains with amorphous carbon shell and magnetic core: Synthesis and their application in removal of heavy metal ions. *Nanoscale* **2011**, *3*, 4600–4603. [CrossRef]
34. Sezgin, Z.; Yüksel, N.; Baykara, T. Preparation and characterization of polymeric micelles for solubilization of poorly soluble anticancer drugs. *Eur. J. Pharm. Biopharm.* **2006**, *64*, 261–268. [CrossRef] [PubMed]

35. Gyulai, G.; Magyar, A.; Rohonczy, J.; Orosz, J.; Yamasaki, M.; Bősze, S.; Kiss, É. Preparation and characterization of cationic Pluronic for surface modification and functionalization of polymeric drug delivery nanoparticles. *Express Polym. Lett.* **2016**, *10*, 216–226. [CrossRef]
36. Pradhan, L.; Srivastava, R.; Bahadur, D. pH- and thermosensitive thin lipid layer coated mesoporous magnetic nanoassemblies as a dual drug delivery system towards thermochemotherapy of cancer. *Acta Biomater.* **2014**, *10*, 2976–2987. [CrossRef] [PubMed]